2010 International Symposium on Nonlinear Theory and its Applications
NOLTA2010, Krakow, Poland, September 5-8, 2010

Analysis of Spike-Trains from Simple Resonate-and-Fire Chaotic Circuit

Satoshi Imai† and Toshimichi Saito†

†EE Dept., Hosei Univ., Tokyo 184-0002, Japan; tsaito AT hosei.ac.jp

Abstract—This paper studies characteristics of inter-spike intervals of simple chaotic spiking neurons having piecewise constant vector field. The circuit repeats vibrate-and-fire dynamics and can output various spike-trains. Using the piecewise exact solution, we can derive the return map and can analyze the dynamics precisely. Using the histogram and recurrence plot of the spike-trains, we classify the characteristics for some key parameters.

1. Introduction

Integrate-and-fire model (IFM) is a simple spiking neuron model. The IFM repeats integrate-and-fire dynamics and can output various spike-trains. The IFM can exhibit synchronous and bifurcation phenomena [1]-[4]. The spiking neuron can be a building-block of pulse-coupled neural networks having rich applications including image processing [5]-[8]. Analysis of spiking neuron models is important to develop bifurcation theory and engineering applications. This paper studies the resonate-and-fire circuit (RFC): our original spiking neuron model having piecewise constant characteristics [4]. Below the threshold, the state variable vibrates divergently around the origin and draws a rect-spiral. If the state variable reaches the threshold, it is reset to the base and the circuit outputs a spike. Repeating the vibrate-and-fire dynamics, the circuit can output various spike-trains. Using the piecewise exact solution, we can derive the return map that enables us to analyze chaos and rich bifurcation phenomena precisely [4]. In this paper, we especially consider the characteristics of spike-trains using three method: histogram of inter-spike-interval (ISI), recurrence plot of the return map orbit (RP1) and RP of the ISI sequence (RP2). The RP is a visualization method of the time series signals [9][10]. Applying them to typical chaotic spike-trains, we can suggest the following:

(1) Using the histogram, we have classified the ISI characteristics into some groups based on wide-band spectrum, line spectrum and their mixture.

(2) Using the RP1 and RP2, we have classified the complex spike-trains and simple spike-trains.

(3) If the burst spike-trains are dominant, the image of the RP1 is different from that of RP2, otherwise the RP1 and RP2 can provide similar images.

2. Resonate-and-Fire Circuit

Fig. 1 shows the RFC. Below the threshold V_T, the dynamics is described by

$$C_1\frac{d}{dt}v_1 = I_2\mathrm{sgn}(v_1+v_2) \quad \text{for } v_1(t) < V_T \qquad (1)$$
$$C_2\frac{d}{dt}v_2 = I_1\mathrm{sgn}(-v_1)$$

$$\mathrm{sgn}(x) = \begin{cases} 1 & \text{for } x > 0 \\ -1 & \text{for } x < 0 \end{cases} \qquad (2)$$

As shown in Fig. 2, if v_1 reaches V_T, the switch S is closed and v_1 is reset to the base E_a instantaneously holding $v_2 = constant$.

$$[v_1(t^+), v_2(t^+)]^T = [E_a, v_2(t)]^T \text{ for } v_1(t) = V_T \qquad (3)$$

Using the dimensionless variables and parameters

$$x = \frac{v_1}{aV_T},\ y = \frac{v_2}{V_T},\ \tau = \frac{I_1 t}{C_2 V_T},\ a = \frac{C_2 I_2}{C_1 I_1},\ q = \frac{E_a}{V_T} \qquad (4)$$

Eqs. (1) and (3) are transformed into

$$\frac{d}{d\tau}x = \mathrm{sgn}(y+ax) \quad \text{for } x(\tau) < 1 \qquad (5)$$
$$\frac{d}{d\tau}y = \mathrm{sgn}(-x)$$

$$[x(\tau^+), y(\tau^+)]^T = [q, y(\tau)]^T \text{ for } x(\tau) = 1 \qquad (6)$$

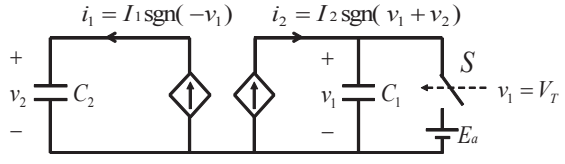

Figure 1: Resonate-and-Fire Circuit

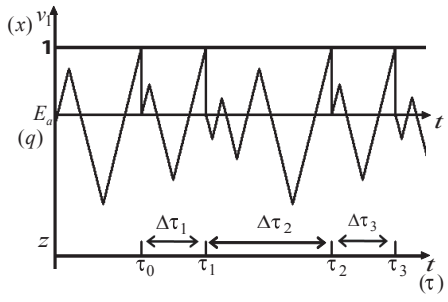

Figure 2: Dynamics of the resonate-and-fire neuron

This system has piecewise constant vector field and characterized by two parameters: damping a and base q. Fig. 2 illustrates a typical waveform. x vibrates divergently below the threshold $x = 1$. If x reaches threshold $x = 1$, x is reset to the base q. Repeating vibrate-and-fire dynamics, the RFC outputs the spike-trains.

Let τ_n be the n-th spiking position and let $\Delta\tau_n = \tau_n - \tau_{n-1}$ be the n-th ISI. Fig. 3 shows typical trajectories. As parameters vary, the RFC can exhibit various spike-trains and typical examples of the ISI histograms are shown in Fig. 4. In Fig. 4(a), the histogram has wide band spectrum. In Fig. 4(b) and (c), the histogram has narrow band spectrum. In Fig. 4(d), the histogram consists of line and continuous spectrums. The RFC can output various spike-trains, however, the histogram-based analysis is not sufficient to classify the ISI characteristic. Hence, we consider the ISI by both histogram and RP in Sec. 4.

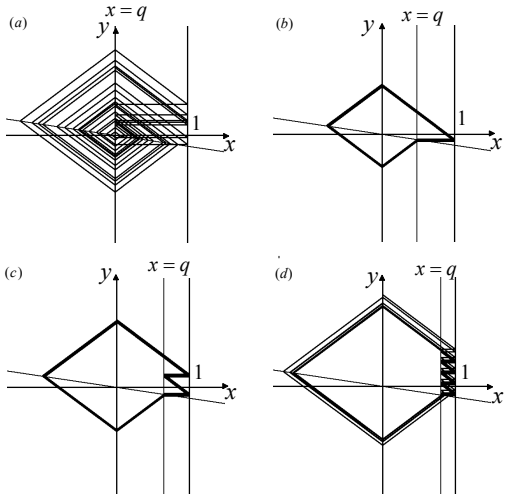

Figure 3: Typical attractor for $a = 0.2$ ((a) chaos for $q = 0$, (b) island for $q = 0.48$, (c) island for $q = 0.65$, (d) chaos for $q = 0.8$)

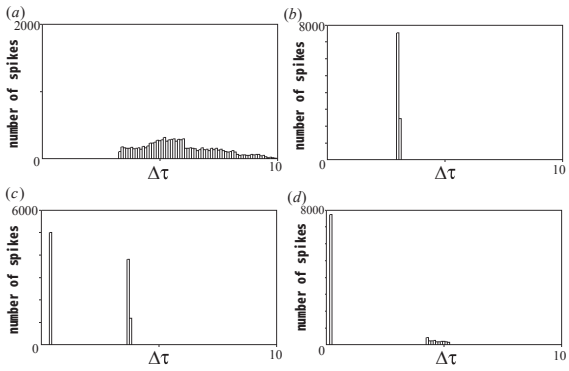

Figure 4: Histogram of the ISI corresponding to Fig. 3 (total number of spikes = 10000, $|bin| = 0.1$, $a = 0.2$ (a) $q = 0$, (b) $q = 0.48$, (c) $q = 0.65$, (d) $q = 0.8$)

3. Return Map

Here, we derive the return map. Fig. 5 shows the key objects. Let $L_q = \{(x, y)|x = q\}$ be the domain of the return map. We consider the trajectory started from point y_0 on L_q. If x reaches the threshold $x = 1$, x jumps the base q. Then trajectory returns to L_q and let y_1 be the return point. Since y_1 is determined by y_0, we can define the return map f from L_q to itself:

$$y_{n+1} = f(y_n) \tag{7}$$

Fig. 6 shows typical return maps corresponding to Fig. 3. In the figure, invariant interval I is shown: an orbit eventually enters into I. In Fig. 6(a), the map has infinite branches in I and exhibits complex chaotic behavior. In Fig. 6(b), the invariant interval I exists near the fixed point. As q increases, the graph moves upward and size of I increases. In Fig. 6(c), we have confirmed that the chaotic orbit can move in the thin period-2 islands.

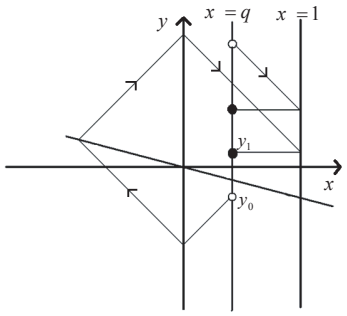

Figure 5: Definition of the return map

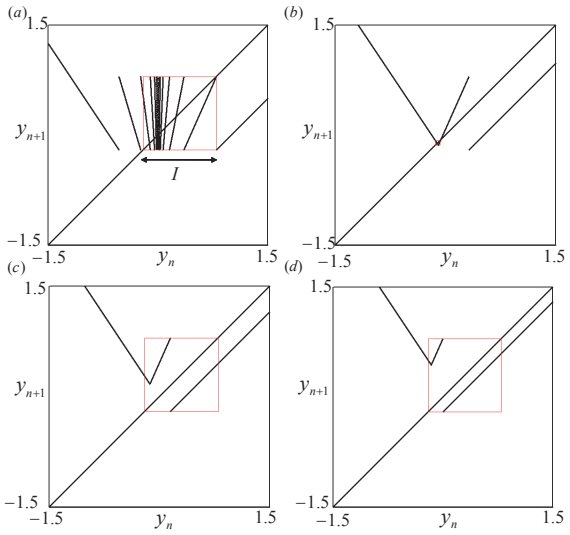

Figure 6: Return map for $a = 0.2$ ((a) chaos for $q = 0$, (b) island for $q = 0.48$, (c) island for $q = 0.65$, (d) chaos for $q = 0.8$)

4. Recurrence Plot

The RP is known as an analyzing method of chaotic dynamics. This method transforms the time series data to two-dimensional graphics. Using the RP, we can visualize time correlation, periodic and chaotic behavior, stationarity and nonstationarity. Using the RP, we consider the classification of the spike-trains of the RFC.

Let us consider the RP for time series data $v(t)$ ($t = 1, 2, \cdots, N$). Let S be a two-dimensional plane of $N \times N$. Calculate the distance $D(i, j)$ between i-th data $v(i)$ and j-th data $v(j)$:

$$D(i, j) = |v(i) - v(j)| \tag{8}$$

If $D(i, j) < \theta$, we plot the (i, j) cell of S, where θ is threshold. Repeating this process for all $D(i, j)$ ($i = 1, 2, \cdots, N$; $j = 1, 2, \cdots, N$), we can make the RP.

We construct the RP for two kinds of data: return map orbits $\{y_0, y_1, \cdots, y_{N-1}\}$ and ISI sequence $\{\Delta\tau_1, \Delta\tau_2, \cdots, \Delta\tau_N\}$. Let D_y and D_{ISI} be the distance calculated for the y data and the ISI data, respectively. Let θ_y and θ_{ISI} be the threshold for RP of the y data and the ISI data, respectively. We plot the (i, j) picture cell, as the following:

For y data

$$D_y(i, j) = |y_i - y_j| < \theta_y \tag{9}$$

For ISI data

$$D_{ISI}(i, j) = |\Delta\tau_i - \Delta\tau_j| < \theta_{ISI} \tag{10}$$

The RPs for y data and ISI data are abbreviated by RP1 and RP2, respectively. Figs. 7 and 8 show the RP1 and RP2 corresponding to the Fig. 3. Figs. 7(a) and 8(a) are complex image, because the RFC outputs complex spike-trains. The y and the ISI data have wide band spectrum. For $q = 0.48$ and 0.65, the chaotic attractors are islands and are similar to periodic attractor, hence the RP becomes monotone as shown in Figs. 7(b), 7(c), 8(b) and 8(c). The RP for period-2-like islands (Figs. 7(c) and 8(c)) has lighter tone than that for period-1-like islands (Figs. 7(b) and 8(b)). Figs. 7(d) and 8(d) exhibit complex image, and we can see RP2 is darker than RP1. In order to consider the difference between RP1 and RP2, we have calculated the plot rate for q as shown in Fig. 9. The rate has the peak around $q = 0.48$ that corresponds to the period-1 islands. The seconds and third peaks correspond to higher-period islands. Note that the difference between RP1 and RP2 increases as q increases from $q = 0.48$ of the first peak. As one reason of the difference, we can say the following: as q increases, the equidistant ISI component and the line spectrum increases, whereas reset points on the base $x = q$ have different y component. y data can have larger variation than the ISI data.

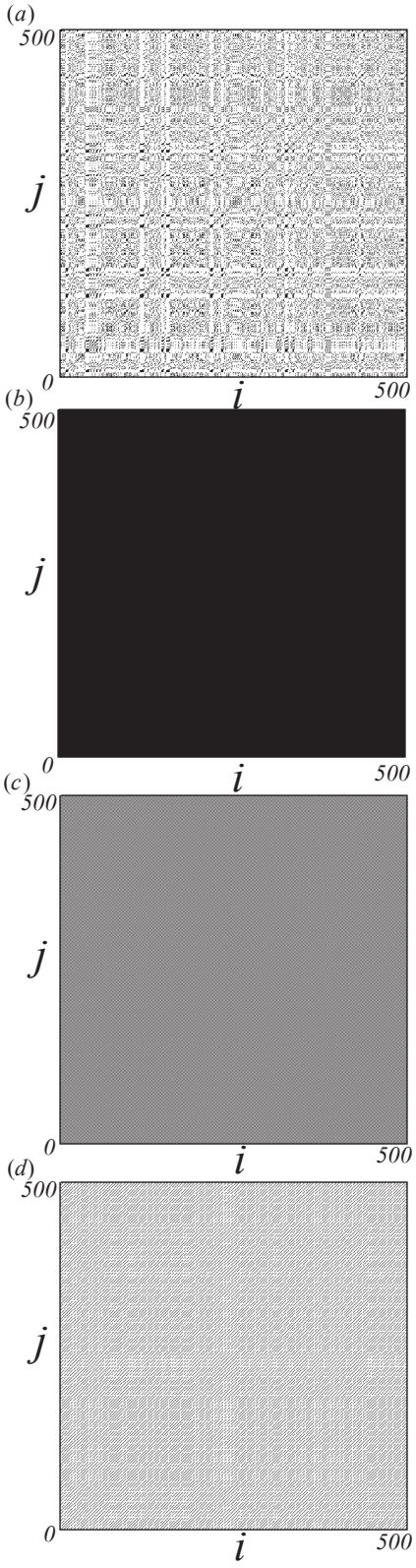

Figure 7: Recurrence plot using y data for $\theta_y = 0.1$, $N = 500$ and $a = 0.2$ ((a) $q = 0$, (b) $q = 0.48$, (c) $q = 0.65$, (d) $q = 0.8$)

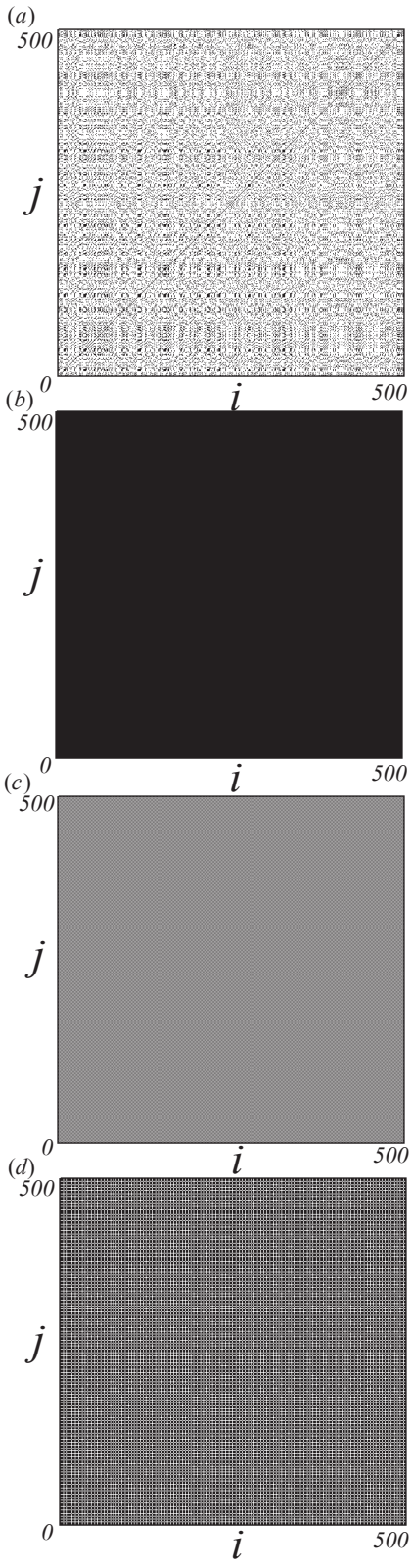

Figure 8: Recurrence plot using the ISI data for $\theta_{ISI} = 0.5$, $N = 500$ and $a = 0.2$ ((a) $q = 0$, (b) $q = 0.48$, (c) $q = 0.65$, (d) $q = 0.8$)

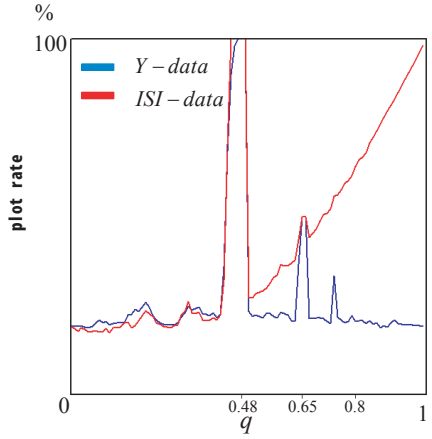

Figure 9: Plot rate of recurrence plot for $\theta_y = 0.1$, $\theta_{ISI} = 0.5$, $a = 0.2$

5. Conclusions

We have analyzed the RFC having various chaotic dynamics. The spike-trains are analyzed using histogram, RP1 and RP2. Using the histogram, we have classified the value of the ISI. Using the RP1 and RP2, we have visualized dynamical property of spike-trains. Especially, the difference between RP1 and RP2 has been considered. Future problems include more detailed analysis of the characteristics of spike-trains for some key parameters and extracting some key measure(s) from the RP.

References

[1] J. P. Keener, F. C. Hoppensteadt, and J. Rinzel, "Integrate-and-fire models of nerve membrane response to oscillatory input," SIAMJ. Appl. Math., vol.41, pp.503-517, 1981

[2] E. M. Izhikevich, "Resonate-and-fire neurons," Neural Netw.,vol.14, pp.883-894, 2001

[3] L. Glass and M. C. Mackey, "A simple model for phase locking of biological oscillators," J. Math. Biology, no.7, pp.339-352, 1979

[4] Y. Matsuoka, T. Hasegawa, and T. Saito, "Chaotic Spike-Train with Line-Like Spectrum," IEICE Trans. Fundamentals, E92-A, 4, pp.1142-1147, 2009

[5] S. R. Campbell, D. Wang, and C. jayaprakash, "Synchrony and desynchrony in integrate-and-fire oscillators," Neural Comput., vol.11, pp.1595-1619, 1999

[6] M. Sushchik, N. Rulkov, L. Larson, L. Tsimring, H. Abarbanel, K. Yao, and A. Volkovskii, "Chaotic pulse position modulation: A robust method of communicating with chaos," IEEE Commun. Lett., vol.4, no.4, pp.128-130, 2000

[7] G. M. Maggio, N. Rulkov, and L. Reggiani, "Pseudo-chaotic time hopping for UWB impulse radio," IEEE Trans. Circuits Syst. I, vol.48, no.12, pp.1424-1435, 2001

[8] H. Nakano, T. Saito, "Grouping Synchronization in a Pulse-Coupled Network of Chaotic Spiking Oscillators," IEEE Trans. Neural Networks, 15, 5, pp.1018-1026, 2004

[9] J. P. Eckmann, S. O. Kamphorst, and D. Ruelle, "Recurrence Plots of Dynamical Systems," Europhysics Letters, 5, pp.973-977, 1987

[10] M. Koebbbe, and G. M. Kress, "Use of recurrence plot in the analysis of Time-Series Data," Nonlinear Modeling and Forecasting, pp.361-378, 1992